JOURNAL OF SYNCHROTRON RADIATION
ISSN 1600-5775

Lead apatites: structural variations among $Pb_5(BO_4)_3Cl$ with B = P (pyromorphite), As (mimetite) and V (vanadinite)

Sytle M. Antao* and Inayat Dhaliwal

Department of Geoscience, University of Calgary, Calgary, Alberta, Canada T2N 1N4.
*Correspondence e-mail: antao@ucalgary.ca

Received 5 July 2017
Accepted 2 October 2017

Edited by A. F. Craievich, University of São Paulo, Brazil

Keywords: lead apatites; pyromorphite; mimetite; vanadinite; structure; chemistry; synchrotron high-resolution powder X-ray diffraction (HRPXRD); Rietveld refinement.

Supporting information: this article has supporting information at journals.iucr.org/s

The crystal structure of four Pb apatite samples, $Pb_5(BO_4)_3Cl$, was refined with synchrotron high-resolution powder X-ray diffraction data, Rietveld refinements, space group $P6_3/m$ and Z = 2. For this isotypic series, B = P^{5+} is pyromorphite, B = As^{5+} is mimetite and B = V^{5+} is vanadinite. The ionic radius for As^{5+} (0.355 Å) is similar to that of V^{5+} (0.335 Å), and this is twice as large as that for P^{5+} (0.170 Å). However, the c unit-cell parameter for mimetite is surprisingly different from that of vanadinite, although their unit-cell volumes, V, are almost equal to each other. No explanation was available for this peculiar c-axis value for mimetite. Structural parameters such as average $\langle B{-}O\rangle$ [4], $\langle Pb1{-}O_9\rangle$ [9] and $\langle Pb2{-}O_6Cl_2\rangle$ [8] distances increase linearly with V (the coordination numbers for the cations are given in square brackets). Mimetite has a short Pb2—O1 distance, so the O1 oxygen atom interacts with the $6s^2$ lone-pair electrons of the Pb^{2+} cation that causes the Cl—Cl distance (= c/2) to increase to the largest value in the series because of repulsion, which causes the c-axis to increase anomalously. Although Pb apatite minerals occur naturally in ore deposits, they are also formed as scaly deposits in lead water pipes that give rise to lead in tap water, as was found recently in Flint, Michigan, USA. It is important to identify Pb-containing phases in water-pipe deposits.

1. Introduction

Apatite is a mineral of interest in various fields because of its importance in geology and technology. Hydroxylapatite, $Ca_5(PO_4)_3(OH)$, is well known in biological sciences because it is the main constituent of dental enamel and human bones. Apatite, $Ca_5(PO_4)_3(OH,F,Cl)$, is the most abundant rock-forming phosphate-group mineral and is the main phosphorous host in crustal rocks (McConnell, 1973).

Lead apatites, $Pb_5(BO_4)_3(Cl)$, where B = P^{5+} is pyromorphite, B = As^{5+} is mimetite and B = V^{5+} is vanadinite, occur in various worldwide localities and as scaly deposits in lead water pipes. Recently, the issue of lead in tap water was highlighted in Flint, Michigan, USA, where high levels of lead were recorded (Robeznieks, 2015). Phosphate is added to drinking water in the UK to minimize the release of lead from lead water pipes (Hopwood *et al.*, 2016). The phosphate addition promotes the formation of insoluble lead apatites on the walls of the water pipes where they occur as scaly deposits. Hydroxylpyromorphite, $Pb_5(PO_4)_3(OH)$, is the lead apatite that is used often to model lead levels in tap water. However, apatites on lead water pipes were shown to be solid solutions between pyromorphite and chlorapatite, $(Ca_{5-x}Pb_x)(PO_4)_3[(OH)_yCl_{1-y}]$ (Hopwood *et al.*, 2016). The structure of a related

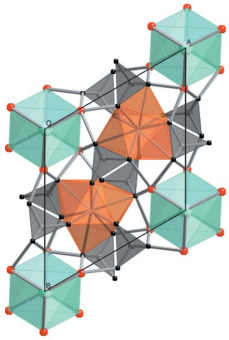

lead apatite mineral, phosphohedyphane, $Ca_2Pb_3(PO_4)_3Cl$, is also known (Kampf *et al.*, 2006). Oscillatory zoning in an arsenate mineral, erythrite, $Co_3(AsO_4)_2{\cdot}8H_2O$, was recently discussed (Antao & Dhaliwal, 2017).

High ion conductivity in rare-earth silicate oxyapatites is of interest (*e.g.* Nakayama *et al.*, 1995, 1999; Ali *et al.*, 2009). Their conductivity at relatively low temperatures is of potential benefit for electrolyte materials in solid oxide fuel cells (Fergus, 2006). There is no rigorous explanation as to why only oxide ions in rare-earth silicate oxyapatites can move freely inside the channel whereas other ions [F, Cl and (OH)] in apatites were found to be localized at the (0,0,0) or (0,0,z) position.

Studies on the crystal chemistry of apatite supergroup minerals began with the determination of the structure of fluorapatite by Mehmel (1930) and Náray-Szabó (1930) and continue to recent times (*e.g.* Okudera, 2013, and references therein). The crystal chemistry of apatites has been described in a few reviews (Elliott *et al.*, 2002; White & Zhili, 2003; Pasero *et al.*, 2010).

Based on other apatite-group minerals, pyromorphite was assumed to have hexagonal space group $P6_3/m$ (Hendricks *et al.*, 1932). The structure was refined to an R-factor of 12% by using visual estimates of intensities from precession photographs (Trotter & Barnes, 1958). The pyromorphite structure was refined with mixed isotropic and anisotropic displacement parameters (Dai & Hughes, 1989). Thereafter, the pyromorphite structure was refined with anisotropic displacement parameters (ADPs) (*e.g.* Akao *et al.*, 1989; Hashimoto & Matsumoto, 1998; Laufek *et al.*, 2006; Mills *et al.*, 2012). The mimetite structure was refined by Calos *et al.* (1990) and that of vanadinite by Laufek *et al.* (2006). The structure of all three Pb apatites, using duplicate samples, was recently refined with ADPs (Okudera, 2013).

The general formula for the lead apatite isotypic series is $Pb_5(BO_4)_3Cl$, Z = 2, space group $P6_3/m$, with B = P^{5+} (pyromorphite), V^{5+} (vanadinite) and As^{5+} (mimetite). In these isomorphs, the O atoms occupy special positions, O1 and O2, and a general position, O3. The divalent Pb1 and Pb2 cation sites are at the 4*f* and 6*h* positions, respectively. The Cl anion occurs at the 2*b* position (0,0,0). The Pb1 site is coordinated by nine O atoms of six BO_4 tetrahedral groups. The Pb2 site is eight-coordinated by six O and two Cl atoms. The Cl atom is octahedrally coordinated by six Pb2 atoms and each O atom is tetrahedrally coordinated by one B and three Pb atoms (Fig. 1). The Pb2 site is commonly found in an off-centred coordination environment in lead-containing apatites (Rouse *et al.*, 1984; Kampf *et al.*, 2006).

In the isotypic Pb apatites, the main difference is in the effective ionic radius (IR) of the B tetrahedral cation (P^{5+} = 0.170, V^{5+} = 0.335, As^{5+} = 0.355 Å and O^{2-} = 1.380 Å; Shannon, 1976). Based on IR, one may expect the unit-cell parameters for the As and V apatites to be nearly equal, but their c parameters are quite different. The reason for this difference is not known. Based on radii sum, one may also expect distances close to the following: P—O = 1.550, V—O = 1.735 and As—O = 1.715 Å. However, experimentally, P—O = 1.542 (8), V—O = 1.710 (12) and As—O = 1.664 (16) Å (Okudera, 2013), so there appears to be significant differences for both the V—O and As—O distances. Based on IR, the unit-cell volume for vanadinite is expected to be slightly smaller than mimetite, but the opposite is found. Moreover, significant differences occur for the c unit-cell parameter between mimetite and vanadinite although the IR for As and V are nearly the same. The reasons for these discrepancies are not clear and will be examined in this study.

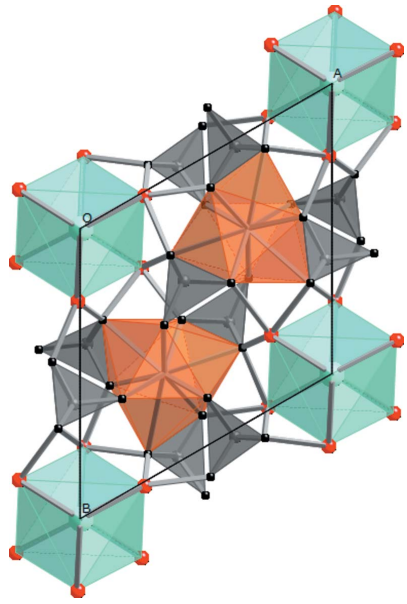

Figure 1
Structure of vanadinite (space group $P6_3/m$) projected down [001]. The structure contains VO_4 tetrahedra (grey) and $Pb1O_9$ polyhedra (orange). The $Pb2O_6Cl_2$ polyhedra are not shown. The Cl atoms (blue) are in the 6_3 channels and form $Cl—Pb2_6$ octahedra (blue). The Pb2 sites are shown in red and O sites in black. The hexagonal unit-cell edges are outlined.

There are some experimental difficulties associated with structure refinements of lead apatites, despite the availability of high-quality museum specimens. X-ray scattering is dominated by highly absorbing Pb atoms among lighter atoms and the interaction of V atoms with neutrons is negligible. As a result, published crystal structure refinements for all Pb apatites contain errors for positional coordinates in the third decimal place for the light O atoms, so errors occur in the second decimal place for bond distances (*e.g.* Flis *et al.*, 2010; Okudera, 2013). Therefore, despite successful structure refinements for Pb apatites, the errors are still large. However, synchrotron high-resolution powder X-ray diffraction (HRPXRD) data were successfully used to refine the crystal structures of Pb-containing materials such as $PbCO_3$ and $PbSO_4$ (Antao & Hassan, 2009; Antao, 2012).

The study examines the crystal structure of Pb apatites (pyromorphite, mimetite and vanadinite) using Rietveld structure refinements and HRPXRD data. The reason for the unusual unit-cell parameter for mimetite is explained based on Cl—Cl repulsion arising from interactions of the O1 atom with the $6s^2$ lone-pair electrons on the Pb^{2+} cation. Structural variations among Pb apatites are discussed.

2. Experimental methods

2.1. Sample locality and description

Experiments were performed on samples of pyromorphite from (1) the Daoping Mine, Gunagxi Province, China, and (2) Ontario, Canada; (3) mimetite from the Pingtouling Mine, Guangdong, China, and (4) vanadinite from Mibladén, Morocco. All samples contain euhedral crystals with well developed faces. The colours of the crystals are (1) pale green, (2) yellow, (3) orange and (4) red. Except for the Ontario sample, single-crystal structure refinements of samples from localities (1), (3) and (4) above were carried out (*e.g.* Laufek *et al.*, 2006; Okudera, 2013). The pyromorphite sample used by Dai & Hughes (1989) was from Globe, Arizona, USA, and their vanadinite was from New South Wales, Australia. A mimetite sample from Durango, Mexico, was studied by Dai *et al.* (1991). Moreover, previous results from single-crystal and Rietveld structure refinements are compared in this study.

2.2. Electron-probe micro-analyzer

Quantitative chemical compositions and back-scattered electron images were collected with a Jeol JXA-8200 WD-ED electron-probe micro-analyzer (EPMA). The Jeol operating program on a Solaris platform was used for ZAF correction and data reduction. The wavelength-dispersive operating conditions were 15 kV accelerating voltage, 20 nA beam current and 5 µm beam diameter. *Kα* radiation and the following standards were used: gallium arsenide (As), vanadium oxide (V), pyromorphite (Pb, P), scapolite (Cl), hornblende (Fe, Na, Ca), cobalt (Co), nickel oxide (Ni), zinc oxide (Zn), barite (Ba) and strontianite (Sr). The EPMA results are listed in Table 1. The chemical composition of the Pb apatite samples are close to their ideal chemical formulae, which were used in previous structure refinements (see, for example, Okudera, 2013).

Table 1
Chemical analyses for Pb apatite samples with formula $M_5(BO_4)_3Cl$.

Wt% sample	(1) Pyromorphite (China)	(2) Pyromorphite (Ontario)	(3) Mimetite (China)	(4) Vanadinite (Morocco)
PbO wt%	82.14	81.56	74.24	78.43
FeO	0.01	0.01	0.00	0.01
CoO	0.01	0.01	0.03	0.00
NiO	0.00	0.03	0.01	0.02
BaO	0.49	0.90	0.17	0.13
ZnO	0.02	0.00	0.05	0.03
CaO	0.08	0.36	0.01	0.01
Na_2O	0.00	0.01	0.01	0.02
SrO	0.00	0.00	0.01	0.00
P_2O_5	15.87	16.09	0.06	0.46
As_2O_5	0.00	0.00	23.01	0.00
V_2O_5	0.03	0.04	0.03	18.72
Cl	2.65	2.68	2.38	2.51
	101.30	101.69	100.01	100.34
$-O\equiv Cl$	0.60	0.60	0.54	0.57
Total	100.70	101.09	99.47	99.77
Numbers of ions on the basis of 16 (M + *B*)				
Pb cations	9.863	9.656	9.912	9.934
Fe	0.002	0.002	0.000	0.004
Co	0.005	0.003	0.012	0.001
Ni	0.001	0.009	0.002	0.008
Ba	0.085	0.155	0.033	0.024
Zn	0.005	0.000	0.020	0.009
Ca	0.039	0.170	0.006	0.002
Na	0.000	0.005	0.012	0.018
Sr	0.000	0.000	0.003	0.000
ΣM	10.000	10.000	10.000	10.000
P	5.991	5.989	0.025	0.180
As	0.000	0.000	5.966	0.000
V	0.009	0.011	0.009	5.820
Σ*B*	6.000	6.000	6.000	6.000
Cl	2.000	2.000	2.000	2.000

2.3. Synchrotron high-resolution powder X-ray diffraction

The samples were studied using HRPXRD that was performed at beamline 11-BM, Advanced Photon Source, Argonne National Laboratory, USA. A small fragment (about 2 mm in diameter) of the sample was crushed to a fine powder using an agate mortar and pestle. The crushed sample was loaded into a Kapton capillary (0.8 mm internal diameter) and rotated during the experiment at a rate of 90 rotations per second. The data were collected at 23°C to a maximum 2θ of about 50° with a step size of 0.001° and a step time of 0.1 s per step. The HRPXRD traces were collected with a unique multi-analyzer detection assembly consisting of 12 independent silicon (111) crystal analyzers and $LaCl_3$ scintillation detectors that reduce the angular range to be scanned and allow rapid acquisition of data. A silicon (NIST 640c) and alumina (NIST 676a) standard (ratio of $\frac{1}{3}Si : \frac{2}{3}Al_2O_3$ by weight) was used to calibrate the instrument and refine the monochromatic wavelength used in the experiment (see Table 2). Additional details of the experimental setup are given elsewhere (Antao *et al.*, 2008; Lee *et al.*, 2008; Wang *et al.*, 2008). Similar experiments were successfully used to examine other minerals (*e.g.* Antao *et al.*, 2002; Antao & Hassan, 2002; Ehm *et al.*, 2007; Skinner *et al.*, 2012).

2.4. Rietveld structure refinements

The HRPXRD traces were modelled using the Rietveld method (Rietveld, 1969), as implemented in the *GSAS* program (Larson & Von Dreele, 2000), and using the *EXPGUI* interface (Toby, 2001). Scattering curves for neutral atoms were used in all refinements. For the structure of Pb apatite, the starting atom coordinates, unit-cell parameters and space group $P6_3/m$ were taken from Hughes *et al.* (1989).

In the *GSAS* program, the reflection-peak profiles were fitted using a type-3 profile (pseudo-Voigt; Caglioti *et al.*, 1958; Thompson *et al.*, 1987). The background was modelled with a Chebyschev polynomial (eight terms). A full-matrix least-

Table 2
HRPXRD data and Rietveld refinement statistical indicators.

	(1) Pyromorphite (China)	(2) Pyromorphite (Ontario)	(3) Mimetite (China)	(4) Vanadinite (Morocco)	(4) − (3)
a (Å)	9.96350 (3)	9.99496 (3)	10.24824 (3)	10.32465 (3)	0.07641 (4)
c (Å)	7.32427 (1)	7.33997 (2)	7.45340 (2)	7.34508 (2)	−0.10832 (3)
V (Å^3)	629.678 (3)	635.019 (3)	677.927 (3)	678.075 (3)	0.148 (4)
Reduced χ^2	1.747	1.548	1.863	1.002	
$R(F^2)$†	0.0774	0.0752	0.0768	0.0541	
Data points	42502	37399	37528	38000	
N_{obs}	1563	1136	1232	1236	
λ (Å)	0.41323 (2)	0.41330 (2)	0.41421 (2)	0.41397 (2)	

† $R(F^2)$ = overall R structure factor based on observed and calculated structure amplitudes = $[\sum(F_o^2 - F_c^2)/\sum(F_o^2)]^{1/2}$. 2θ range = 2.5–40.0°. Sample (1) is more crystalline than sample (2), so it has a much larger N_{obs} value, and the errors for the structural parameters are much smaller.

squares refinement varying a scale factor, unit-cell parameters, zero shift, atom coordinates and isotropic displacement parameters converged rapidly. The number of data points and the number of observed reflections in the HRPXRD trace for each sample are given in Table 2. Synchrotron powder X-ray diffraction patterns are shown in Fig. 2. Table 2 contains the Rietveld refinement statistical indicators and unit-cell parameters. The atom coordinates are given in Table 3. Some site occupancy factors were refined and those for the O atoms were fixed (Table 3). Selected bond distances and angles are given in Table 4.

Table 3
Atom coordinates†, isotropic displacement parameters ($U \times 10^2$ Å^2) and site occupancy factors (sofs).

Site		(1) Pyromorphite (China)	(2) Pyromorphite (Ontario)	(3) Mimetite (China)	(4) Vanadinite (Morocco)
Pb1	x	1/3	1/3	1/3	1/3
	y	2/3	2/3	2/3	2/3
	z	0.0039 (2)	0.0051 (2)	0.0066 (2)	0.0071 (1)
	U	1.04 (1)	2.40 (2)	1.31 (2)	1.37 (1)
	sof	0.948 (5)	1.0	1.02 (1)	0.948 (9)
Pb2	x	0.25449 (7)	0.25475 (8)	0.25099 (6)	0.25512 (5)
	y	0.0055 (1)	0.0059 (1)	0.00500 (9)	0.01238 (7)
	U	1.04 (1)	2.34 (1)	1.42 (1)	1.43 (1)
	sof	0.959 (5)	1.0	1.02 (1)	0.946 (9)
B	x	0.4093 (4)	0.4099 (5)	0.4081 (1)	0.4096 (2)
	y	0.3773 (4)	0.3803 (5)	0.3838 (1)	0.3838 (2)
	U	0.77 (9)	1.5 (1)	0.70 (4)	0.46 (8)
	sof	1.0	1.0	1.04 (1)	0.94 (1)
O1	x	0.3426 (9)	0.3450 (9)	0.3207 (8)	0.3317 (9)
	y	0.4905 (8)	0.4919 (9)	0.4927 (8)	0.4979 (8)
	U	1.0 (2)	2.4 (3)	1.0 (3)	2.7 (3)
O2	x	0.5898 (9)	0.5886 (9)	0.6007 (9)	0.5984 (8)
	y	0.4778 (9)	0.4741 (9)	0.4873 (8)	0.4842 (8)
	U	1.1 (3)	1.7 (3)	2.0 (3)	1.6 (3)
O3	x	0.3639 (6)	0.3598 (8)	0.3591 (6)	0.3561 (6)
	y	0.2755 (6)	0.2698 (8)	0.2730 (6)	0.2686 (6)
	z	0.0784 (6)	0.0813 (8)	0.0649 (8)	0.0636 (7)
	U	1.6 (2)	3.0 (2)	3.9 (3)	2.1 (2)
Cl	U	1.2 (1)	1.4 (1)	1.4 (1)	1.2 (1)
	sof	0.95 (1)	1.0	0.99 (1)	0.94 (1)

† Cl is at (0, 0, 0) and z = 1/4 for Pb2, B, O1 and O2. B = P (pyromorphite), As (mimetite) and V (vanadinite). The sofs for the O atoms were fixed at 1. The sofs for the other atoms were either refined or fixed at 1.0.

3. Results and discussion

3.1. Structure of Pb apatites

This study reports Rietveld structure refinements of Pb apatite samples from some classical localities. Other researchers have also used samples from these localities, so the results from several studies can be compared. Pyromorphite and mimetite samples from China and vanadinite from Mibladén, Morocco, were also examined by other researchers (Laufek *et al.*, 2006; Okudera, 2013). These studies reported the ideal chemical formulae $Pb_5(BO_4)_3Cl$ based on EPMA results and the ideal formulae were used in their structure refinements. In this study, some site occupancy factors (sofs) were refined (Table 3). Our sofs agree well with our EPMA results.

The crystal structure of Pb apatite is shown in Fig. 1. The Pb1 site is surrounded by nine O atoms, and the Pb2 site is surrounded by six O atoms and two Cl atoms. The B site is surrounded by four O atoms. The bond distances and angles of the two pyromorphite samples are in good agreement (Table 4). The distortions in the BO_4 tetrahedra are similar to each other.

The structure of Pb apatite isotypes is similar to those previously reported. The minerals crystallize with the chlorapatite structure, space group $P6_3/m$, and the Cl atom occurs at the 2b position with no evidence of site splitting. The Pb2 site is commonly found in an off-centric coordination environment (Rouse *et al.*, 1984; Kampf *et al.*, 2006).

The bond-valence sums (BVS) for the Pb^{2+} and B^{5+} cations are close to their formal valences (Table 4). The BVS value for Cl^- is close to 1.0 valence unit (v.u.) for mimetite and vanadinite, but it is 1.16 v.u. for pyromorphite (Table 4). BVS values higher than 1.25 v.u. for Cl^- were calculated for phosphohedyphane, $Ca_2Pb_3(PO_4)_3Cl$ (Kampf *et al.*, 2006), $Sr_2Ba_3(AsO_4)_3Cl$ (Đordević *et al.*, 2008), synthetic alforsite, $Ba_5(PO_4)_3Cl$ (Hata *et al.*, 1979), and lower than 1.1 v.u. in $Sr_5(VO_4)_3Cl$ (Beck *et al.*, 2006).

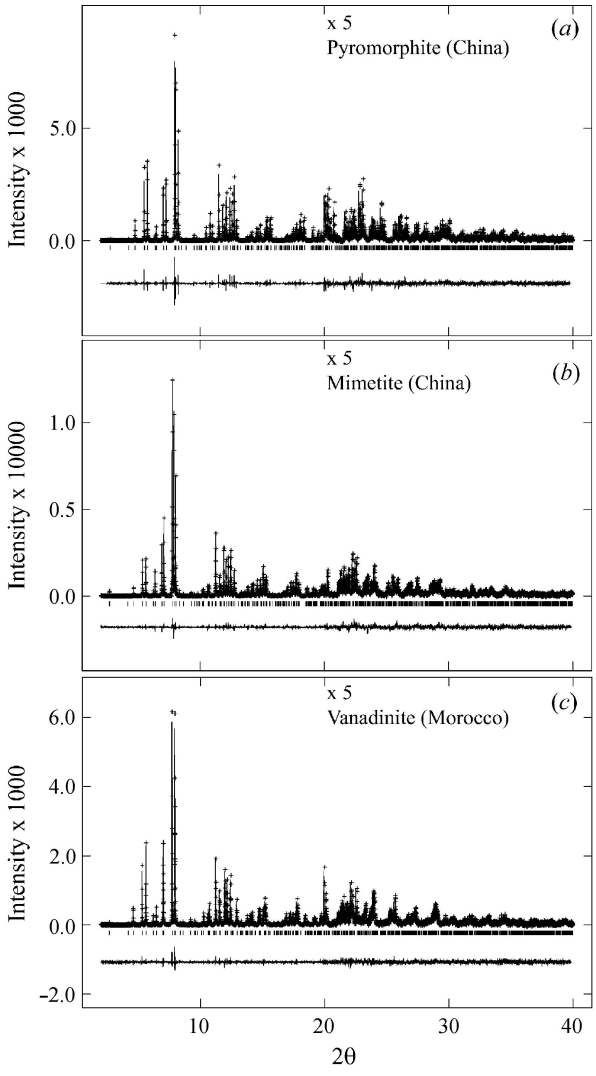

Figure 2
Comparison of HRPXRD traces at 23°C for Pb apatites: (*a*) pyromorphite, (*b*) mimetite and (*c*) vanadinite together with the calculated (continuous line) and observed (crosses) profiles. The difference curve ($I_{obs} - I_{calc}$) with the same intensity scale is shown at the bottom of the trace. Short vertical lines indicate allowed reflection positions. The intensities for the trace and difference curve that are above 20° 2θ are multiplied by 5. The intensity scale for mimetite is ten times those for the other samples.

3.2. Variations among unit-cell parameters in Pb apatites

The relationships between unit-cell parameters are shown in Fig. 3. Data from the literature are included for comparison (see Fig. 3 and its caption for references). The unit-cell parameters fall along two straight lines representing the P–As and As–V apatite series. The volumes for mimetite and vanadinite are almost equal. However, vanadinite has the largest *a* unit-cell parameter (Fig. 3*a*). The *c* parameter for mimetite is significantly larger than that for vanadinite, which is nearly the same as that for pyromorphite (Fig. 3*b*). The *c*/*a* ratio for mimetite is larger than that for vanadinite (Fig. 3*c*). Pyromorphite and vanadinite have similar values for the *c* parameter, but that for mimetite is the largest (Fig. 3*d*). All unit-cell data from the literature seem reasonable, including single-crystal data, so there appears to be no difficulties in obtaining good unit-cell parameters.

The unit-cell parameters occur in three groups, which may indicate limited solid solutions in nature. However, this observation may arise from the small number of natural samples examined. The unit-cell parameters of the synthetic samples show complete solid solutions between the pyromorphite–mimetite series (Flis *et al.*, 2010). Although complete solid solutions may be possible along the mimetite–vanadinite and pyromorphite–vanadinite joins, unit-cell data are needed for synthetic samples along these joins. In nature, solid solutions occur to a very limited extent, so samples from different localities have similar unit-cell parameters that cluster in three groups. Why is the *c* parameter between mimetite and vanadinite so different (0.108 Å), whereas the effective ionic radii difference between As (0.335 Å) and V (0.355 Å) is quite small (Δc = 0.020 Å)? In contrast, the *c* parameter between pyromorphite and mimetite differ by a similar amount (Δr = 0.113 Å), but the effective ionic radii difference between P (0.170 Å) and As (0.335 Å) is quite large (0.165 Å). The answer to this question is based on the significant differences between mimetite and vanadinite and is related to the Cl—Cl and Pb2—O1 distances, as explained below.

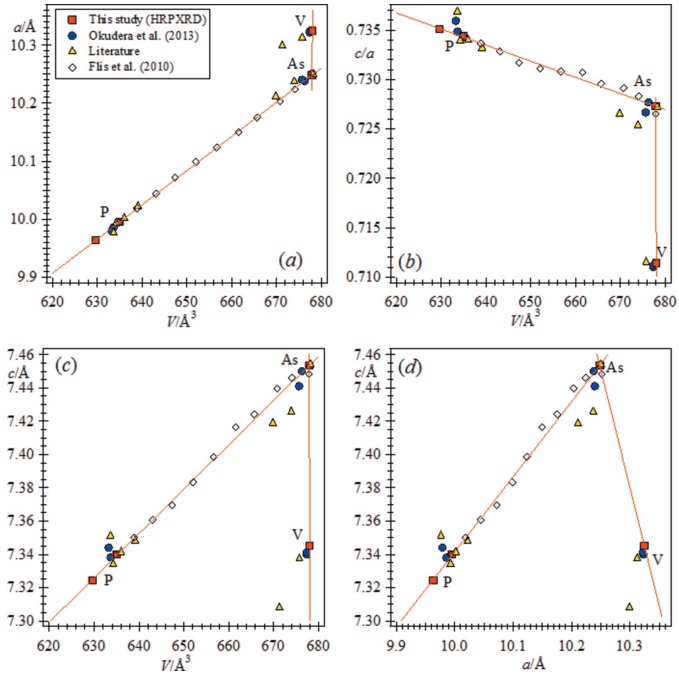

Figure 3
Unusual relationships among unit-cell parameters. (*a*) Non-linear relations occur between *a* and *V*. *V* is nearly the same for mimetite and vanadinite, but the latter has the largest *a* parameter. (*b*) The *c* parameter for mimetite is larger than that for vanadinite, which is nearly the same as that for pyromorphite. (*c*) Pyromorphite has the largest *c*/*a* parameter. (*d*) Pyromorphite and vanadinite have a similar *c* parameter, but that for mimetite is the largest. Our data for the pyromorphite sample from China have the smallest *V*, which is different from other studies for samples from this locality. Unit-cell data shown as yellow triangles are from the literature (Dai & Hughes, 1989; Calos *et al.*, 1990; Dai *et al.*, 1991; Hashimoto & Matsumoto, 1998; Laufek *et al.*, 2006; Sejkora *et al.*, 2011; Mills *et al.*, 2012).

Table 4
Pb apatites: selected bond distances (Å) and angles (°).

BVS was calculated with the program *VaList* (A. S. Wills), which is available from http://www.ccp14.ac.uk.

	(1) Pyromorphite (China)	(2) Pyromorphite (Ontario)	(3) Mimetite (China)	(4) Vanadinite (Morocco)	(4) − (3)
Pb1—O1 × 3	2.550 (6)	2.550 (7)	2.501 (5)	2.488 (5)	−0.013 (7)
Pb1—O2 × 3	2.687 (6)	2.682 (8)	2.769 (6)	2.754 (6)	−0.015 (8)
Pb1—O3 × 3	2.839 (5)	2.875 (7)	2.942 (6)	2.976 (5)	0.034 (8)
⟨Pb1—O⟩ [9]	2.692 (1)	2.702 (1)	2.737 (1)	2.739 (1)	0.002 (1)
BVS	2.09	2.06	1.99	2.01	
Pb2—Cl × 2	3.1058 (4)	3.1150 (5)	3.1558 (3)	3.1606 (4)	0.005 (4)
Pb2—O1	3.078 (8)	3.112 (11)	3.016 (7)	3.194 (8)	0.178 (11)
Pb2—O2	2.326 (8)	2.362 (10)	2.334 (8)	2.349 (7)	0.015 (11)
Pb2—O3 × 2	2.659 (5)	2.612 (7)	2.763 (6)	2.684 (5)	−0.079 (8)
Pb2—O3′ × 2	2.627 (5)	2.646 (6)	2.577 (6)	2.556 (5)	−0.021 (8)
⟨Pb2—O⟩ [6]	2.663 (3)	2.665 (3)	2.672 (3)	2.671 (2)	−0.001 (4)
⟨Pb2—O,Cl⟩ [8]	2.773 (2)	2.778 (3)	2.793 (2)	2.793 (2)	0.000 (3)
BVS	2.00	1.98	1.92	1.96	
B—O1	1.569 (9)	1.545 (13)	1.745 (7)	1.727 (8)	−0.018 (11)
B—O2	1.560 (8)	1.547 (10)	1.711 (8)	1.690 (7)	−0.021 (11)
B—O3 × 2	1.534 (5)	1.565 (7)	1.695 (6)	1.714 (5)	0.019 (8)
⟨*B*—O⟩ [4]	1.549 (3)	1.556 (5)	1.712 (3)	1.711 (3)	0.000 (5)
BVS	4.82	4.73	4.67	5.14	
O1—*B*—O2	107.8 (5)	109.7 (7)	113.9 (4)	111.7 (4)	−2.2 (6)
O1—*B*—O3 × 2	112.6 (3)	114.1 (4)	110.7 (2)	112.0 (2)	1.3 (3)
O2—*B*—O3 × 2	106.8 (3)	107.0 (4)	106.2 (2)	107.4 (2)	1.2 (3)
O3—*B*—O3′	110.0 (4)	104.5 (6)	108.9 (4)	106.1 (4)	−2.8 (6)
⟨O—*B*—O⟩ [6]	109.42	109.40	109.43	109.43	0.0
BVS for Cl	1.16	1.13	1.02	1.01	
Cl—Cl (= *c*/2)	3.66213 (1)	3.66999 (1)	3.72670 (1)	3.67254 (1)	−0.054

Our two pyromorphite samples have different unit-cell parameters. The sample from Ontario has unit-cell data that coincide with that of the synthetic end-member, but the other sample from China has the smallest *V*, which indicates subtle chemical differences between the two samples (Table 1).

3.3. Structural variations in Pb apatites

Linear variations of selected distances with the unit-cell volume, *V*, are shown in Fig. 4. The average ⟨Pb1—O⟩ [9] distances increase linearly with *V* (Fig. 4*a*). The Pb2—Cl distance also increases linearly with *V* (Fig. 4*b*). The Cl—Cl distance (= *c*/2) increases linearly with the *c* parameter, as expected (not shown). Both the average ⟨Pb2—O⟩ [6] and ⟨Pb2—O_6,Cl_2⟩ [8] distances increase linearly with *V* [Figs. 4(*c*) and 4(*d*)]. The average ⟨*B*—O⟩ distance also increases linearly with *V* (Fig. 4*e*). Both mimetite and vanadinite have similar structural parameters because the radii for As and V are nearly the same (Fig. 4*f*).

A regular tetrahedron has six equal angles of 109.47°. Across the series, the O—*B*—O angles do not vary in a systematic manner. However, their average ⟨O—*B*—O⟩ [6] angle is close to the regular tetrahedron value (Table 4).

Some discrepancies are clearly observed between the present data and those from the literature (Fig. 4). Okudera (2013) selected two crystals from each of his three samples and presented six data points (duplicate runs). Chemical analyses of crystals from the same sample are not variable, so the differences observed between his duplicate samples arise only from experimental errors. This is clearly observed for some parameters shown for mimetite and vanadinite [Figs. 4(*c*) and 4(*d*)]. Other data from the literature, indicated by triangles, are off the red trend lines for data from this study, especially for pyromorphite [Figs. 4(*c*) and 4(*d*)]. For the synthetic samples along the pyromorphite–mimetite join [Figs. 4(*a*), 4(*c*) and 4(*d*)], the structural data fall on black trend lines that are different from the red trend lines of this study.

In Table 4, differences between mimetite and vanadinite are shown. The largest difference is between their *c* unit-cell parameter, Pb2—O1, and Cl—Cl distances. The Pb2—O1 distance is short in mimetite, whereas the Cl—Cl (= *c*/2) distance is long. The opposite is observed for vanadinite where the Pb2—O1 distance is long and the Cl—Cl distance is short.

The coordination of the Pb2 site in vanadinite is shown together with the distances within the Pb2—O_6Cl_2 polyhedra (Fig. 5). A large open space exists between the two Cl and O1 oxygen atoms where the $6s^2$ lone-pair electrons on the Pb^{2+} cation occurs (Kampf *et al.*, 2006). As Pb2—O1 becomes shorter, the $6s^2$ lone-pair electrons move towards the two Cl atoms and cause them to move apart because of Cl—Cl repulsion. The opposite is the case for vanadinite. This feature explains the different and unusual *c* unit-cell parameters for mimetite and vanadinite, as discussed above.

From a structural point of view, solid solutions are expected among pyromorphite, mimetite and vanadinite (Figs. 3 and 4). However, synthetic samples for the various joins are needed and the structure of such samples needs to be well characterized. An analysis of compositions of natural members of the pyromorphite–mimetite–turneaureite–chlorapatite system suggests the existence of a complete solid solution among

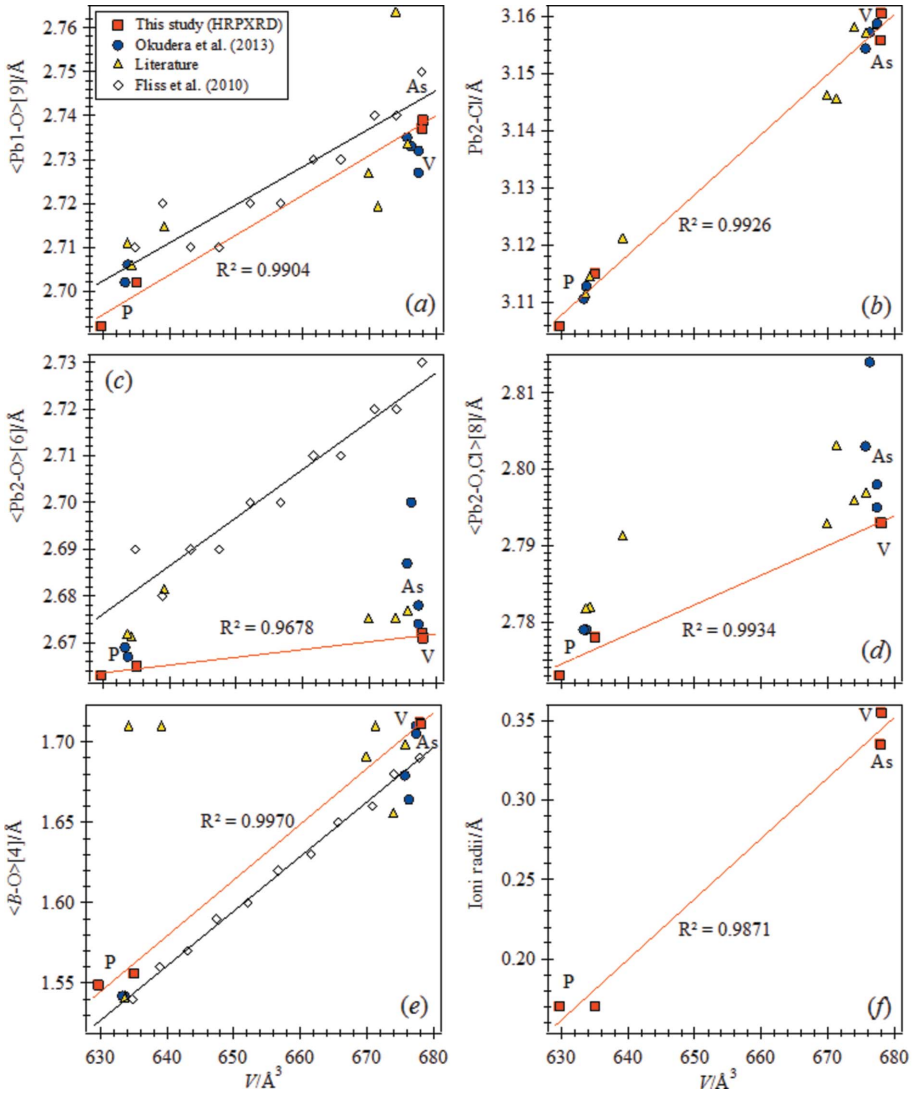

Figure 4
Linear variations of structural parameters. (*a*) The average ⟨Pb1—O⟩ [9] distances increase linearly with *V*. (*b*) The Pb2—Cl distance increases linearly with *V*. The (*c*) average ⟨Pb2—O⟩ [6] and (*d*) ⟨Pb2—O_6,Cl_2⟩ [8] distances increase linearly with *V*. (*e*) The average ⟨*B*—O⟩ distance and (*f*) effective ionic radii (Shannon, 1976) increase linearly with *V*. Mimetite and vanadinite have similar structural parameters. Some discrepancies are observed between the present data and some of those from the literature, especially for the ⟨*B*—O⟩ distance from Hashimoto & Matsumoto (1998) and average ⟨Pb2—O⟩ [6] and ⟨Pb2—O,Cl⟩ [8] distances from Okudera (2013). Structural data shown as yellow triangles are from the literature (Dai & Hughes, 1989; Calos *et al.*, 1990; Dai *et al.*, 1991; Hashimoto & Matsumoto, 1998; Laufek *et al.*, 2006; Sejkora *et al.*, 2011; Mills *et al.*, 2012).

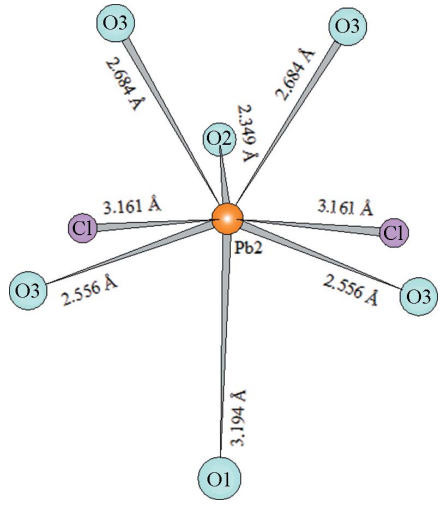

Figure 5
The coordination of the Pb2 site in vanadinite. The distances within the Pb2—O_6Cl_2 polyhedra are given. The Pb2—O1 distance is shortest in mimetite and the Cl—Cl (= *c*/2) distance is the longest, whereas the opposite is observed for vanadinite. Between the two Cl and O1 atoms is a large open space where the $6s^2$ electron lone pair on the Pb^{2+} cation occurs. As Pb2—O1 becomes shorter, the $6s^2$ lone-pair electrons move towards the two Cl atoms and cause them to move apart because of repulsion. The opposite is the case for vanadinite. This feature explains the different *c* unit-cell parameters for mimetite and vanadinite.

pyromorphite, mimetite, hedyphane and phosphohedyphane [$Ca_2Pb_3(PO_4)_3Cl$]. No stable solid solutions appear to exist between the joins phosphohedyphane–hedyphane and chlorapatite–turneaureite in natural systems (Kampf *et al.*, 2006).

Calcian pyromorphite has been identified as the major lead-bearing phase in mine waste soils from the South Pennine orefield, UK (Cotter-Howells *et al.*, 1994), and the Carterhouse mine in the Mendip Hills, UK (Cotter-Howells & Caporn, 1996). In experiments on the use of apatite amendments to Pb-contaminated soil (including associated grass roots) from a residential area near Oakland, California, USA, Laperche *et al.* (1997) noted that, when the soils were treated with phosphate rock (containing fluorapatite as the major constituent), all pyromorphite formed contained significant Ca. The apparent stability in natural systems of members of the chlorapatite–pyromorphite series between pyromorphite and phosphohedyphane, but not between phosphohedyphane and chlorapatite, may have important implications for the use of apatite to reclaim Pb-contaminated waters and soils.

This study shows that HRPXRD is a powerful technique that can be used to obtain reliable structural parameters on gem-quality crystals that diffract poorly. Moreover, highly penetrating synchrotron X-rays can also be used to study samples that contain strongly absorbing atoms.

Acknowledgements

We thank the two anonymous reviewers and the Co-editor, A. F. Craievich, for useful comments that helped to improve this manuscript. R. Marr is thanked for his help with the electron probe. The HRPXRD data were collected at the X-ray Operations and Research beamline 11-BM, Advanced

Photon Source, Argonne National Laboratory, USA. Use of the Advanced Photon Source was supported by the US Department. of Energy, Office of Science, Office of Basic Energy Sciences, under Contract No. DE-AC02-06CH11357.

Funding information

Funding for this research was provided by: Natural Sciences and Engineering Research Council of Canada (grant to SMA).

References

Akao, A., Aoki, H., Innami, Y., Minamikata, S. & Yamada, T. (1989). *Rep. Inst. Med. Dent. Eng. Tokyo Med. Dent. Univ.* **23**, 25–29.
Ali, R., Yashima, M., Matsushita, Y., Yoshioka, H. & Izumi, F. (2009). *J. Solid State Chem.* **182**, 2846–2851.
Antao, S. M. (2012). *Am. Mineral.* **97**, 661–665.
Antao, S. M. & Dhaliwal, I. (2017). *Minerals*, **7**, 136.
Antao, S. M., Duane, M. J. & Hassan, I. (2002). *Can. Mineral.* **40**, 1403–1409.
Antao, S. M. & Hassan, I. (2002). *Can. Mineral.* **40**, 163–172.
Antao, S. M. & Hassan, I. (2009). *Can. Mineral.* **47**, 1245–1255.
Antao, S. M., Hassan, I., Wang, J., Lee, P. L. & Toby, B. H. (2008). *Can. Mineral.* **46**, 1501–1509.
Beck, H. P., Douiheche, M., Haberkorn, R. & Kohlmann, H. (2006). *Solid State Sci.* **8**, 64–70.
Caglioti, G., Paoletti, A. & Ricci, F. P. (1958). *Nucl. Instrum.* **3**, 223–228.
Calos, N. J., Kennard, C. H. L. & Davis, R. L. (1990). *Z. Kristallogr.* **191**, 125–129.
Cotter-Howells, J. D. & Caporn, S. (1996). *Appl. Geochem.* **11**, 335–342.
Cotter-Howells, J. D., Champness, P. E., Charnocky, J. M. & Pattrick, R. A. D. (1994). *Eur. J. Soil Sci.* **45**, 393–402.
Dai, Y. & Hughes, J. M. (1989). *Can. Mineral.* **27**, 189–192.
Dai, Y., Hughes, J. M. & Moore, P. B. (1991). *Can. Mineral.* **29**, 369–376.
Đordević, T., Šutović, S., Stojanović, J. & Karanović, Lj. (2008). *Acta Cryst.* C**64**, i82–i86.
Ehm, L., Antao, S. M., Chen, J. H., Locke, D. R., Marc Michel, F., David Martin, C., Yu, T., Parise, J. B., Antao, S. M., Lee, P. L., Chupas, P. J., Shastri, S. D. & Guo, Q. (2007). *Powder Diffr.* **22**, 108–112.
Elliott, J. C., Wilson, R. M. & Dowker, S. E. P. (2002). *Adv. X-ray Anal.* **45**, 172–181.
Fergus, J. W. (2006). *J. Power Sources*, **162**, 30–40.
Flis, J., Borkiewicz, O., Bajda, T., Manecki, M. & Klasa, J. (2010). *J. Synchrotron Rad.* **17**, 207–214.
Hashimoto, H. & Matsumoto, T. (1998). *Z. Kristallogr.* **213**, 585–590.
Hata, M., Marumo, F., Iwai, S. & Aoki, H. (1979). *Acta Cryst.* B**35**, 2382–2384.
Hendricks, S. B., Jefferson, M. E. & Mosley, V. M. (1932). *Z. Kristallogr.* **81**, 352–369.
Hopwood, J. D., Derrick, G. R., Brown, D. R., Newman, C. D., Haley, J., Kershaw, R. & Collinge, M. (2016). *J. Chem.* **2016**, 9074062.
Hughes, J. M., Cameron, M. & Crowley, K. D. (1989). *Am. Mineral.* **74**, 870–876.
Kampf, A. R., Steele, I. M. & Jenkins, R. A. (2006). *Am. Mineral.* **91**, 1909–1917.
Laperche, V., Logan, T. J., Gaddam, P. & Traina, S. J. (1997). *Environ. Sci. Technol.* **31**, 2745–2753.
Larson, A. C. & Von Dreele, R. B. (2000). *General Structure Analysis System (GSAS)*. Report LAUR 86–748. Los Alamos National Laboratory, New Mexico, USA.
Laufek, F., Skála, R., Haloda, J. & Cisařová, I. (2006). *J. Czech. Geol. Soc.* **51**, 271–275.
Lee, P. L., Shu, D., Ramanathan, M., Preissner, C., Wang, J., Beno, M. A., Von Dreele, R. B., Ribaud, L., Kurtz, C., Antao, S. M., Jiao, X. & Toby, B. H. (2008). *J. Synchrotron Rad.* **15**, 427–432.
McConnell, D. (1973). *Apatite: Its Crystal Chemistry, Mineralogy, Utilization, and Geologic and Biologic Occurrences.* New York: Springer-Verlag.
Mehmel, M. (1930). *Z. Kristallogr.* **75**, 323–331.
Mills, S. J., Ferraris, G., Kampf, A. R. & Favreau, G. (2012). *Am. Mineral.* **97**, 415–418.
Nakayama, S., Kageyama, T., Aono, H. & Sadaoka, Y. (1995). *J. Mater. Chem.* **5**, 1801–1805.
Nakayama, S., Sakamoto, M., Higuchi, M., Kodaira, K., Sato, M., Kakita, S., Suzuki, T. & Itoh, K. (1999). *J. Eur. Ceram. Soc.* **19**, 507–510.
Náray-Szabó, S. (1930). *Z. Kristallogr.* **75**, 387–398.
Okudera, H. (2013). *Am. Mineral.* **98**, 1573–1579.
Pasero, M., Kampf, A. R., Ferraris, C., Pekov, I. V., Rakovan, J. & White, T. J. (2010). *Eur. J. Mineral.* **22**, 163–179.
Rietveld, H. M. (1969). *J. Appl. Cryst.* **2**, 65–71.
Robeznieks, A. (2015). *Mod. Healthc.* **45**, 9.
Rouse, R. C., Dunn, P. J. & Peacor, D. R. (1984). *Am. Mineral.* **69**, 920–927.
Sejkora, J., Plášil, J., Císařová, I., Škoda, R., Hloušek, J., Veselovský, F. & Jebavá, I. (2011). *J. Geosci.* **56**, 257–271.
Shannon, R. D. (1976). *Acta Cryst.* **32**, 751–767.
Skinner, L. B., Benmore, C. J., Antao, S. M., Soignard, E., Amin, S. A., Bychkov, E., Rissi, E., Parise, J. B. & Yarger, J. L. (2012). *J. Phys. Chem. C*, **116**, 2212–2217.
Thompson, P., Cox, D. E. & Hastings, J. B. (1987). *J. Appl. Cryst.* **20**, 79–83.
Toby, B. H. (2001). *J. Appl. Cryst.* **34**, 210–213.
Trotter, J. & Barnes, W. H. (1958). *Can. Mineral.* **6**, 161–173.
Wang, J., Toby, B. H., Lee, P. L., Ribaud, L., Antao, S. M., Kurtz, C., Ramanathan, M., Von Dreele, R. B. & Beno, M. A. (2008). *Rev. Sci. Instrum.* **79**, 085105.
White, T. J. & ZhiLi, D. (2003). *Acta Cryst.* B**59**, 1–16.